VNUHCM Journal of Science and Technology Development 2026, 29(3):4231-4243

Open Access Full Text Article

Research Article

Enhancing printed circuit board defect detection: combining optical systems and deep learning

Hieu Dau Sy[1], Phuc Dang Thi[2,*], Thuan Tran Minh[1]

ABSTRACT

The increasing complexity and miniaturization of electronic devices have heightened the need for high-quality PCB inspection to ensure product reliability and functionality. This study proposes a deep learning-based detection system supported by a custom-designed optical setup using coaxial illumination to deliver high-contrast images with clearly highlighted defects. The data were collected from faulty PCBs during production and enriched via various augmentation techniques, including the creation of artificial defects, to enhance the diversity of the dataset. The enhanced YOLOv8 framework was evaluated with multiple backbone configurations—YOLOv8+1P, ResNet152, HRNet, HRDnet+2 backbone, and HRDnet+3 backbone—achieving test accuracies of 92, 88, 90, 93.5, and 93.8%, respectively. The results indicate that HRNet and the HRDnet+3 backbone significantly improve the detection of small and blurry defects, with HRDnet+3 providing enhanced deployment efficiency for real-time industrial inspection systems.

Key words: PCB Defect Detection, Optical System, Deep Learning, YOLOv8, ResNet152, HRNet, HRDnet

[1]*Faculty of Applied Science, Ho Chi Minh City University of Technology (HCMUT), Vietnam National University Ho Chi Minh City, 268 Ly Thuong Kiet Street, Dien Hong Ward, Ho Chi Minh, Vietnam*

[2]*Department of Computer Science, Faculty of Information Technology, Industrial University of Ho Chi Minh City, 12 Nguyen Van Bao Street, Hanh Thong Ward, Ho Chi Minh, Vietnam*

Correspondence

Phuc Dang Thi, Department of Computer Science, Faculty of Information Technology, Industrial University of Ho Chi Minh City, 12 Nguyen Van Bao Street, Hanh Thong Ward, Ho Chi Minh, Vietnam

Email: phucdt@iuh.edu.vn

History

- Received: 14-08-2025
- Revised: 27-02-2026
- Accepted: 15-03-2026
- Published Online: 07-09-2026

DOI : 10.32508/vnuhcmj-std.v29i3.4569

INTRODUCTION

Printed circuit board (PCB) manufacturing is prone to various defects, such as incorrect soldering, insufficient or excessive solder, solder bridging, uneven soldering, surface cracks, fractures, and improper electrical connections [1,2]. These defects are often small and subtle, making manual inspection challenging and error prone. Furthermore, in high-volume production, defect detection becomes labor-intensive, time-consuming, and costly. Conventional approaches, such as flying probe testing, can identify electrical faults such as open and short circuits but require significant operational effort and expenses [3]. Consequently, vision-based inspection methods have attracted attention due to their ability to automate and improve the efficiency of defect detection [4,5]. Automated optical inspection (AOI) not only increases accuracy but also reduces labor costs compared to manual inspection [6]. However, effective automated inspection demands both a well-designed optical system to highlight subtle defects and robust algorithms capable of recognizing various defect types across different PCB designs [7].

Despite the progress in PCB defect detection, existing datasets and algorithms face certain limitations. While numerous PCB defect datasets have been developed, employing various acquisition methods and lighting conditions [8–10], variations in PCB types and illumination introduce algorithmic complexity, and limited dataset sizes restrict model generalization [11,12]. Likewise, while approaches ranging from principal component analysis (PCA) [13], image subtraction [14], and normalized cross-correlation [15] to heuristic optimization [16] have shown promise, they often struggle with subtle defects or require extensive preprocessing. More recent machine learning and deep learning-based methods—such as beta-variational autoencoders (beta-VAE) [17], support vector machines (SVMs) [18], CNN-based pose detection [19], VGG16-based classification [20], Transformer–YOLO [21], Extended FPN [22], Faster R-CNN [23], TDD-Net [24], and YOLO variants [25]—have demonstrated high accuracy but still rely heavily on the quality of input images.

In this paper, we address these limitations by improving both the data collection process and the defect detection algorithm. First, we design a customized optical system employing a coaxial lighting technique to optimize the illumination and imaging conditions, enabling the high-contrast visualization of surface anomalies. Second, we enhance the dataset diversity by capturing high-resolution PCB images during production, introducing controlled defects, and applying image-based augmentation. Third, we integrate and fine-tune state-of-the-art deep learning architectures, including YOLOv8 [26], DarkNet [27], ResNet152 [28], HR-

Cite this article : Dau Sy H, Dang Thi P, Tran Minh T. **Enhancing printed circuit board defect detection: combining optical systems and deep learning**. *VNUHCM J. Sci. Technol. Dev.* 2026; 29(3):4231-4243.

Net[29], and HRDNet[30], to achieve high detection precision for small and blurred defects.

The main contributions of this work are as follows:

- Co-designed optical acquisition and detection framework: We design a customized coaxial illumination system combined with a 12MP monochrome camera (12 μm/pixel resolution) to enhance surface defect contrast in industrial PCB inspection. The co-design between optical acquisition and the detection architecture improves the quality of the input image and the overall system performance.
- Industrial-oriented PCB dataset:
- Task-adaptive optimization of YOLO architecture:
- Industrial AOI validation:

The paper is structured into three main sections. The introduction provides an overview of the problem, the adopted approach, and relevant previous research. The methodology encompasses the proposed techniques for designing an optical system for PCBs to ensure efficient input images, along with suggested deep learning models for identifying errors on PCBs. The experimental results present the input data, training outcomes on various models, evaluation, and comparison of the findings. The conclusions summarize the findings and suggest future research directions. The optical system design—a tailored coaxial lighting setup combined with a 12MP monochrome camera—achieves a 12 μm/pixel resolution and significantly improves defect contrast:

- Dataset Diversity—A rich and diverse dataset is built from real defective PCBs, supplemented with artificial defects and augmentation techniques.
- Deep Learning Integration—Multiple architectures are fine-tuned for PCB defect localization and classification, achieving high accuracy for challenging cases.
- Practical Implications—The proposed system supports faster and more reliable quality control in electronic manufacturing, enhancing product reliability.

The remainder of the paper is organized as follows. Section 2 reviews related works on PCB defect datasets and presents the proposed methodology, including the optical system, dataset preparation, and deep learning models. Section 3 details the experimental setup, results, and comparative analysis. Section 4 provides a brief discussion, and Section 5 concludes the paper and outlines future research directions.

METHODS

To address the limitations of early PCB defect datasets, recent research has focused on developing publicly available, high-resolution datasets to serve as benchmarks for algorithm evaluation and comparison.

The HRIPCB dataset, proposed by Huang et al.[31], contains 1,386 images from 10 PCB types across six defect categories. Notably, it has been widely used for classification tasks, achieving up to 96% accuracy with deep learning models[32]. Further, the DeepPCB dataset, comprising 1,500 annotated images of six defect types, has been employed by Sanli et al.[33] in combination with a pyramid pooling module, achieving 98% accuracy. In another study, Feng et al.[34] further combined DeepPCB with PKU-Market-PCB to train a CNN–Transformer hybrid model, yielding 81% accuracy.

Despite these advances, challenges remain due to variations in PCB designs and imaging conditions and the limited scale of existing datasets, all of which highlight the need for greater data diversity and optimized image acquisition systems to ensure robust and generalizable detection.

Optical System Design

Various lighting techniques have been employed in PCB inspection systems, including bright-field, dark-field, and coaxial lighting[35]. For objects such as PCBs, which can be considered samples of structural complexity, lighting techniques may include bright-field, dark-field, or coaxial illumination.

For PCBs ranging from 50–200 mm in each dimension, the primary inspection requirements include evaluating the circuitry and surface of the coating layers at the pre-component placement stage and checking for component placement errors and defects arising during the soldering process of completed PCBs.

Given these requirements, the main lighting techniques typically used for illuminating PCB surfaces are bright-field and dark-field illumination (Figure 1). Bright-field lighting is a technique in which illumination is evenly distributed over the inspection area or directed through it in the case of transparent surfaces (Figure 1). The contrast in the resulting image is generated by the inherent structures and color variations on the sample surface. This method is widely used in standard inspection systems, though its effectiveness depends on controlling the direction of light shed onto the surface.

For surfaces with strong reflectivity and rough structures, such as aluminum foil layers on medical or

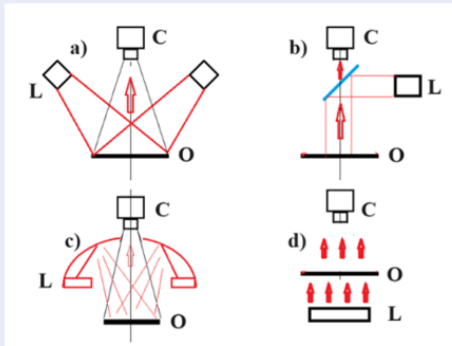

Figure 1: Lighting techniques for product appearance inspection: a) bright field, b) coaxial lighting, c) dome lighting, d) back lighting for transparent samples; C – camera, L – lighting, O – object.

food packaging, the dome lighting technique provides a uniform light field with countless directions and equivalent intensity, ensuring consistent illumination and minimizing glare (Figure 2).

Figure 2: Image of the aluminum foil package containing a disposable surgical scalpel captured by: Smartphone camera with ambient light source (A and C), Mono camera with coaxial lighting technique (B), and Dome lighting (D)

However, for surfaces with high planarity or structured, orderly details (PCBs) where reflectivity is high, a coaxial lighting source directed perpendicularly onto the sample surface can be effectively employed. In this configuration, the reflected light from the surface is highly oriented; this results in greater image contrast and sharper edge definition compared to dome lighting, in which the light returning to the camera predominantly arises due to surface scattering[36].

This paper highlights the advantages of coaxial lighting for PCB inspection. Also known as coaxial illumination, this technique directs light along the same optical axis as the camera lens; this ensures that reflected light returns directly to the lens, minimizing shadows and enhancing the visibility of surface features. It delivers uniform illumination across the PCB surface, producing clear, well-defined images for defect detection. PCBs contain components of varying sizes and shapes arranged per design; capturing effective inspection images requires clear contrast between regions, distinct component outlines, separation between adjacent contours, and the visibility of defects such as cracks, fractures, and deformations. Coaxial lighting directs light uniformly and perpendicularly onto the PCB; this allows reflected rays to form images unaffected by neighboring components, while the defect areas produce varied intensities based on the morphology and material. This makes it ideal for building high-quality training data and deploying robust models. We integrate coaxial lighting with image processing and machine learning to detect anomalies—surface scratches, missing components, damaged pins, and faulty parts—highlighted effectively by this technique. The experimental results indicate that combining a customized optical system with machine learning models is particularly advantageous for PCBs with intricate designs or dense layouts, improving overall quality control in electronics manufacturing.

Deep Learning Models for PCB Defect Detection

The proposed deep learning models for object recognition in this paper are typically categorized into two main objectives. The first objective focuses on achieving high accuracy, requiring sufficiently deep models to extract precise information for identifying small and complex objects. Models ranging from low to high resolution, such as VGG19[37], ResNet[38], Inception[38], EfficientNet[39], HRNet[29], and Transformer[40], are proposed for medical and industrial applications and other domains. However, a drawback of these models is their relatively large network architecture, which can reduce efficiency when deployed in systems. The second objective aims to balance accuracy and real-time deployment capabilities. Models such as Faster-RCNN[20], SSD[41], RetinaNet[42], and YOLO[21] have been proposed for this purpose. These models are designed to handle real-time requirements with lighter network architectures, ensuring the system's real-time performance. However, these models are limited in the sense that their accuracy may not be fully guaranteed in the recognition of complex and challenging objects. Among these models, YOLO stands out due to its outstanding performance in simultaneous object recognition and bounding box delineation (one-stage). Thus, in this paper, we propose the YOLO model for object recognition and bounding box delineation. Additionally, we enhance the model's backbone by improving ResNet 152, HRNet, and HRDNet to increase its accuracy.

You Only Look Once (YOLO)

YOLO was first introduced by Redmon et al. in 2015[27] as a rapid single-stage detector that divides an image into grids to directly predict classes and bounding boxes. Since then, many improved versions have been released[43,44]. In this work, we adopt YOLOv8[26,45], the most recent Ultralytics model for object detection, classification, and instance segmentation.

YOLOv8 features a lightweight backbone and an anchor-free head. Compared with YOLOv5, it replaces C3 with C2f blocks, adjusts early convolution layers ($6\times6 \rightarrow 3\times3$), removes several redundant Conv layers, and simplifies the bottleneck to improve efficiency. The unified head merges the YOLOv5 neck and head, removes anchor boxes, and employs three detection scales with SiLU activation. Glenn Jocher has also introduced a revised objectness-loss formulation to account for scale-dependent object influences[26].

Overall, YOLOv8 offers stronger feature extraction and faster inference than previous YOLO versions, making it well suited for high-performance PCB defect detection. Further, YOLOv8 uses an anchor-free detection head with scale-aware objectness weighting and employs Complete IoU (CIoU) for bounding-box regression (Equation 1):

$$L_{obj} = 4 \times L_{obj}^{small} + 1 \times L_{obj}^{medium} + 0.4 \times L_{obj}^{large} \quad (1)$$

The Complete IoU Loss is described by Equations 2 to 4:

$$L_{CIoU} = 1 - IoU + \frac{p^2(b,b^{gt})}{c^2} + \alpha v \quad (2)$$

$$v = \frac{4}{\pi^2}\left(arc\tan\left(\frac{\omega^{gt}}{h^{gt}}\right) - arc\tan\left(\frac{\omega}{h}\right)\right)^2 \quad (3)$$

$$\alpha = \frac{v}{(1-IoU)+v'} \quad (4)$$

Here, b and b^{gt} represent the centroids of the predicted box and the ground truth box, p denotes the Euclidean distance between the two box centroids, c is the length of the diagonal of the smallest enclosing region that can contain both the predicted and ground truth boxes, α is a positive balancing parameter, and v is used to measure the consistency of the aspect ratio. ω^{gt} and h^{gt} are the width and height of the ground truth box, respectively, and ω and h are the width and height of the predicted box, respectively.

YOLOv8 performs well for many image and real-time video recognition tasks. However, in regard to PCB defect detection, which requires the identification of small and complex objects, its feature extraction may not be ideal. This is because YOLO uses a relatively compact backbone based on EfficientNet. To improve its ability to detect small objects, we suggest several enhancements: increasing the backbone depth to make it more suitable for the data; using or replacing the backbone with models that can extract smaller and more detailed features from images; combining backbones running in parallel at different resolutions; and designing a new backbone that matches the original model, data type, and image resolution.

Improved backbone models of YOLOv8

Increasing the Depth of the YOLOv8 Backbone (YOLOv8+1P): In the standard YOLOv8 backbone, there are five P-blocks, and the network is designed for input images with dimensions of 640×640. After feature extraction in each P-block, the feature map depth is doubled while its spatial resolution is halved. YOLOv8 employs P3, P4, and P5 blocks for object detection. In PCB defect detection, however, input images acquired from our optical system have dimensions of 1518×1518, approximately twice the size used in the original configuration of YOLOv8. To improve the model's feature extraction capacity for such high-resolution inputs, we increase the backbone depth by incorporating additional P-blocks and using P4, P5, and P6 for object detection.

ResNet152 Backbone Integration: The residual neural network (ResNet), introduced by Microsoft Research in 2015[28], represents an architectural milestone in image recognition. Deep neural networks often suffer from the vanishing gradient problem when increasing depth, which degrades the accuracy and impedes training. ResNet addresses this issue by introducing residual connections, enabling direct information flow from earlier to later layers and mitigating gradient vanishing. This significantly improves both the training stability and model accuracy, making ResNet one of the most influential models in deep learning[46]. ResNet152, consisting of 152 layers (Figure 3), offers substantial feature extraction capabilities. To leverage these advantages, we replace the original YOLOv8 backbone with ResNet152, creating a hybrid architecture (Figure 3) that enhances image feature extraction for PCB defect detection.

HRNet: The high-resolution network (HRNet), proposed in 2019 by researchers from Vietnam National University (VNU) and the University of Hong

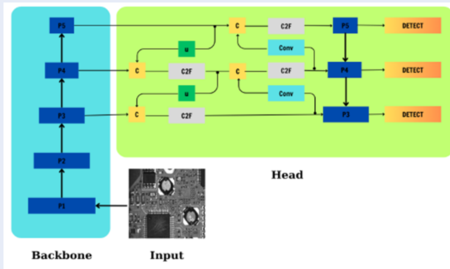

Figure 3: Architecture of model YOLOv8

Kong[29], offers significant improvements in image recognition and has achieved notable success across various computer vision tasks[47]. Unlike traditional models such as ResNet, which reduce the input size through layers and risk feature loss, HRNet maintains high-resolution features throughout processing. Its architecture runs high- and low-resolution layers in parallel, allowing features from different resolutions to complement each other. The network is organized into multiple stages: stage 1 processes high-resolution features; and from stage 2 onward, lower-resolution, deeper features are generated, while high-resolution features from earlier stages are preserved and enriched. This multi-resolution fusion retains detailed spatial information and enhances the semantic representation, improving accuracy. The combined YOLOv8–HRNet architecture is depicted in Figure 4.

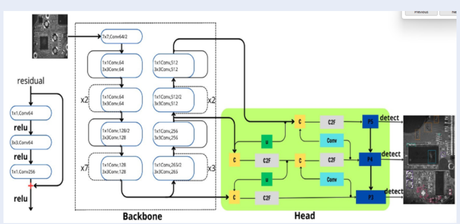

Figure 4: Architecture of model YOLOv8 combines with ResNet152

HRDNet: Proposed in 2020 by Ziming Liu, Guangyu Gao, Lin Sun, and Zhiyuan Fang[30], HRDNet consists of two main components: the multi-depth image pyramid network (MD-IPN) and the multi-scale feature pyramid network (MS-FPN). MD-IPN extracts features from high-resolution images while balancing performance across small, medium, and large objects. MS-FPN integrates contextual information among these multi-scale feature groups. HRDNet also increases the depth of both the backbone and the feature pyramid network (FPN) in parallel, enabling each to extract independent features from different image resolutions before feature fusion and recognition. This design has shown a high performance experimentally; the architecture is illustrated in Figure 5.

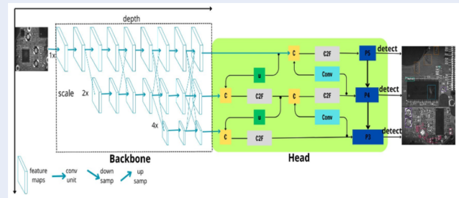

Figure 5: Architecture of model YOLOv8 combine with HRNet

HRDNet With Three Backbones: To further enhance multi-scale feature representation for PCB defect detection, we integrate a three-backbone variant of HRDNet into YOLOv8. The architecture consists of three parallel branches operating at different effective resolutions, enabling richer high-resolution feature extraction while preserving deep semantic information.

The primary backbone (S_0) follows the standard downsampling hierarchy to produce feature maps at strides 8, 16, and 32, corresponding to *P3*, *P4*, and *P5*. Two auxiliary backbones, S_1 and S_2, operate in parallel and generate additional high-resolution features. These branches are aligned via resolution adjustment (upsampling/downsampling), followed by channel-wise concatenation and convolutional refinement to ensure feature consistency.

The fused multibranch representations are injected into the intermediate pyramid levels (notably *P3* and *P4*) before entering the PAN-FPN neck, and the final detection head utilizes the aggregated *P3*–*P 5* outputs for prediction. This three-backbone design strengthens small-object representations and the preservation of fine details while maintaining compatibility with the standard YOLOv8 detection pipeline. The overall structure is illustrated in Figure 5.

HRDNet With Two Backbones: We propose a two-backbone variant of HRDNet to reduce computational costs while preserving multi-scale feature extraction. Rather than employing three parallel backbones on 1518×1518 images with resolution scaling factor , we remove the shallow three P-block branch and retain the two deeper backbones with five and four P-blocks to maintain a strong multi-resolution representation.

The modified HRDNet backbone produces three feature levels corresponding to strides 8, 16, and 32. The feature maps at resolutions *H/8*, *H/16*, and *H/32* are used as *P3*, *P4*, and *P5*, with channel dimensions of 256, 512, and 1024, respectively. Multibranch fusion is implemented via resolution alignment (nearest-neighbor upsampling), followed by channel concatenation and convolutional refinement to unify the feature dimensions.

The resulting {*P3*, *P4*, *P5*} features are fed into the standard YOLOv8 PAN-FPN neck for top-down and bottom-up aggregation before the detection head. The architecture of the proposed two-backbone structure is illustrated in Figure 6.

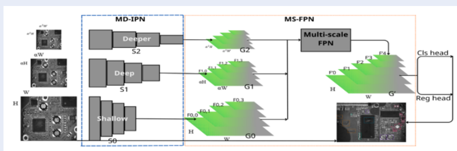

Figure 6: Architecture of model HRDNet

Evaluation of the model

Deep learning models can be evaluated using different standards depending on the task[48,49]. Common metrics include the following:

Accuracy—Ratio of correct predictions to the total evaluation set; useful but less reliable for imbalanced datasets

Precision—Ratio of true positives to all predicted positives for a class, indicating the model's predictive confidence

Recall—Ratio of true positives to all actual positives for a class, reflecting the model's ability to detect all relevant instances

***F* 1-score**—Harmonic mean of precision and recall

The $F1$-score, calculated as in Equation 5, measures the per-class accuracy and overall model performance by combining precision and recall:

$$F1_{score} = 2 \times \frac{precision \times recall}{(precision \times recall)} \quad (5)$$

The mean Average Precision **(mAP)** is widely used in object detection, calculated as the mean of AP values across classes, where AP is the area under each class's precision–recall curve. It reflects the model's precision–recall trade-off across all classes.

The choice of backbones in this work was driven primarily by the need to reliably detect very small and visually subtle defects rather than by extreme model compactness. We, therefore, selected ResNet152 and HRNet48 as strong high-capacity baselines with well-established performance on fine-grained recognition tasks. Building on these, the HRDNet-based variants were designed to retain most of the small-object sensitivity of HRNet while significantly reducing computational cost (only 3.8–4.1 x 10^6 parameters and 10.1 GFLOPs in our YOLOv8 + HRDNet-2 backbone configuration). While lightweight families such as MobileNet, ShuffleNet, and CSPDarkNet are attractive for deployment on significantly resource-constrained devices, our primary industrial use case targets GPU-equipped AOI systems on production lines, where the proposed trade-off between accuracy and computational load is more critical than achieving the smallest possible model size**.**

EXPERIMENTAL RESULTS

Creating a Dataset Using a Specialized Optical System

Optical systems

Figure 7 depicts the real optical system, where the PCB is positioned beneath the lighting module, with the inspection area aligned within the field of view (FOV) of the camera–lens system. The light head's working distance and illumination center were calibrated to ensure uniform brightness across the inspection area, which can be verified using an A4 sheet placed at the PCB position. In this study, a 12 MP (4024 $\times$ 3036 pixels) monochrome camera with a 25-mm focal length lens was used. The camera–lens working distance was determined by the target FOV; in this research, a 55.0 $\times$ 41.5 mm FOV requires a working distance of 105.0 mm. This setup achieves a resolution of 13.6 μm/pixel, enabling the reliable detection of defects as small as 50 μm. The high resolution also improves the clarity of component boundaries, reducing labeling errors during dataset preparation.

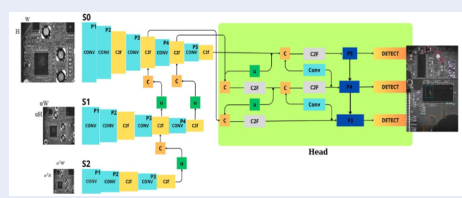

Figure 7: Architecture of YOLOv8 combined with 3 backbone HRDnet

The dataset includes two PCB types—(i) populated boards with components and (ii) unpopulated (bare) boards—as shown in Figure 8. For populated boards, the focus is on component-related defects arising during assembly, inspection, or in-service operation, such as PCB surface scratches, component scratches, missing or lost components, damaged pins (bent, broken, or deformed), and faulty components (incorrect type, defective, or out of specification). For bare boards, defects primarily originate from the fabrication and pre-assembly processes, including excess solder; solder shorts/bridging; and mechanical substrate issues, such as surface scratches, cracks, and edge chipping.

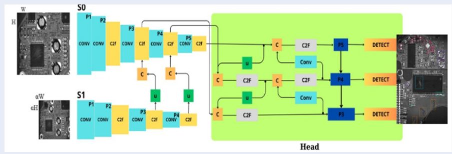

Figure 8: Architecture of YOLOv8 combine with 2 backbone HRDnet

In a production environment, ambient lighting and minor mechanical tolerances can potentially affect the image quality. In our setup, the coaxial illumination head and camera–lens assembly were mounted in a rigid mechanical frame and enclosed to minimize interferences from ambient light. Small variations in the LED intensity over time were compensated for by periodic gain calibration of the camera and monitoring a reference patch on the PCB panel. Our internal tests, with slight changes in the ambient illumination and sub-millimeter deviations in PCB placement, did not produce any noticeable degradation in defect visibility, mainly because the coaxial configuration directs the dominant portion of the illumination along the camera axis and suppresses off-axis reflections.

From a maintenance standpoint, the optical module was installed as a rigid unit comprising the camera, lens, and coaxial light head on a single mounting plate. During deployment, the PCB conveyor was mechanically referenced to this module such that the FOV and working distance remained fixed. In routine operation, only a simple daily check is required: operators place a reference PCB or a uniform white sheet at the inspection position and verify that the overall brightness and focus match the stored template. Recalibration of the working distance or alignment is only needed after mechanical interventions such as replacement of the camera, lens, or light head. This design minimizes the need for frequent calibration while preserving consistency in the optical quality on the production line.

Dataset

All images were captured using the same optical setup described earlier (12 MP monochrome camera, 25-mm lens; FOV = 55.0 × 41.5 mm; working distance = 105 mm; coaxial illumination) under fixed distance and lighting conditions and standardized to 1518 × 1518 px. Given that defect patterns differ between populated and bare PCBs, and to allow for flexible defect recognition across product lines, we created two separate datasets.

Bare PCBs: The base dataset contains 1,000 images (front: 666; back: 334). To increase the diversity, we applied data augmentation, including random rotation (-30° to $+30^\circ$), multidirectional translation (1–25% of the image size), intensity and color adjustments, scaling (75–125%), and composite transformations. Additionally, a subset of defect samples was manually generated in Photoshop to provide clear labels and reduce annotation ambiguity. Augmentation yielded an expanded dataset of 3,500 images. The defect types are illustrated in Figure 9, and their quantities are listed in Table 1.

Table 1: Description of the data collected.

Label	Description	Quantity
0	Insufficient solder	1,182
1	Excess solder	1,544
2	Solder bridging	1,120
3	Board scratches	1,343
4	Cracks/chipping causing trace opens	1,235

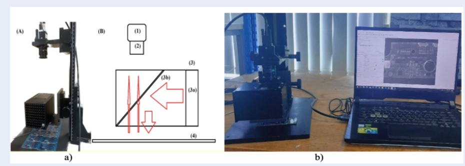

Figure 9: a) The optical system includes: (A) Real optical system. (B) Structure of the optical system: (1) Mono camera, (2) Optical lens,(3) Coaxial light-head: (3a) LED plate, (3b) Semi-coating mirror, (4) object (PCB). b) The optical system when connected to software, producing high-quality images.

Populated PCBs: Typical defects include scratches on the board, scratches on components, damaged component pins, missing/misplaced components, and faulty components. In total, 4,121 images were available, with 3,493 for training, 496 for validation, and 132 for testing. We performed random rotations/translations followed by noise reduction—removing duplicates, images with unclear defects, and frames containing many ($\geq$ 20) identical objects—to mitigate bias. The defect types are presented in Figure 10, and the quantity of each is detailed in Table 2.

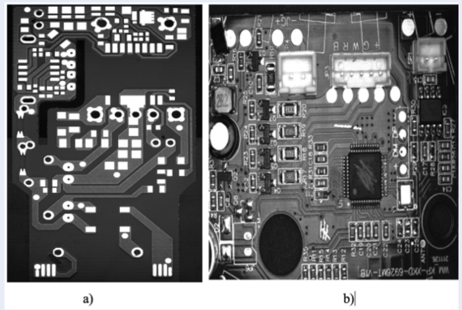

Figure 10: Coaxial-illumination images of PCB surfaces: a) bare (unpopulated) board and b) populated board.

Table 2: Description of the data collected.

Label	Description	Quantity
0	Scratches on the circuit boar	5,791
1	Scratches on components	3,578
2	Missing/lost component	10,880
3	Damaged component pins	5,376
4	Faulty components	4,226

PCB Defect Detection From the Deep Learning Model

The models were trained on Google Colab using the following machine configuration: a CPU with two cores at 2401 MHz, 4GB RAM, and a Tesla T4 GPU with 15GB VRAM. The dataset was divided into training (70%), validation (15%), and testing (15%) sets.

Defect Recognition Results on Bare PCBs: The training results are presented in Table 3. The results for the bare PCB dataset indicate that the backbone has a pronounced impact on performance and computational costs: the baseline YOLOv8 is lightweight but offers limited detection effectiveness, whereas HRNet/ResNet substantially improves the mAP at the expense of an increased number of parameters. Among the upgraded variants, ResNet152 achieves superior recall (better defect coverage), while ResNet152+connected attains a higher mAP and precision, reflecting a bias toward specificity and fewer false positives. Considering the overall metrics alongside the computational expense, ResNet152+connected offers the optimal performance–efficiency balance and is, therefore, the most suitable choice for automated quality inspection. The recognition results are shown in Figure 11.

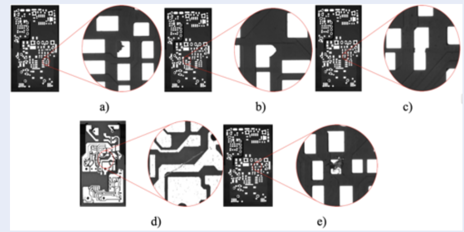

Figure 11: Types of defects on PCB: a) Insufficient solder; b) Excess solder; c) Solder bridging ; d) Board-scratches; e) Cracks/chipping causing trace opens.

Defect Recognition Results on Populated PCBs: The training was performed with a training dataset of 3,493 samples, a validation dataset of 364 samples, a test dataset of 132 samples, and a total of 50 training epochs. Table 4 presents the training results. The sizes of the enhanced models exhibit differences in the number of parameters. The original YOLOv8 model has the smallest size; however, its ability to detect small errors and similarities is unsatisfactory. In contrast, the proposed models have larger sizes. The HRNet48 and ResNet152 models, with deep network architectures, result in relatively heavy model sizes. Leveraging the advantage of deep network structures, these models demonstrate excellent feature extraction capabilities, leading to high accuracy, with the HRNet48 model achieving the highest accuracy. Table 4 also indicates that the sizes of the HRDNet+2 backbone, HRDNet+3 backbone, and YOLOv8+1P models increase insignificantly. The HRDNet model, comprising a lightweight network structure, attains relatively good accuracy, with minimal deviation compared to the HRNet48 model.

The models were evaluated on the test set, with the results presented via the metrics in Table 5. The test set results indicate improved accuracy across the proposed models, with the HRNet and HRDNet+2 backbone models achieving the highest accuracy and exhibiting negligible differences. These results also demonstrate that the model enhancements display increased accuracy and efficiency compared to the original YOLOv8 version. The improved models successfully identify small, complex errors and similarities. Notably, the combined YOLOv8 and HRDNet+2 backbone model proves highly effective in terms of both accuracy and model size. This enhancement, despite increasing the training and deployment

Table 3: Results on the bare PCB dataset.

Backbone	Head	Parameters (M)	Epochs	Precision (%)	Recall (%)	mAP0.5 (%)	GFLOP
YOLOv8 original	YOVOv8	3.2	50	56	33	21.6	8.2
HRNet48	YOVOv8	67	50	89	68	54	271.6
ResNet152	YOVOv8	61	50	89	88	60	196.6
ResNet152+connected	YOVOv8	61,3	50	90	68	65	196.7

Table 4: Results on the populated PCB dataset.

Backbone	Head	Parameters (M)	Epochs	Precision (%)	Recall (%)	mAP0.5 (%)	GFLOP
YOLOv8 original	YOVOv8	3.2	50	91	85	91	8.2
YOLOv8-1P	YOVOv8	4	50	92	87	92.5	4.8
HRNet48	YOVOv8	67	50	94	88	94	271.6
ResNet152	YOVOv8	61	50	89	88	92	196.6
HRDnet-3backbone	YOVOv8	4.1	50	91	89	92.8	10.5
HRDnet-2backbone	YOVOv8	3.8	50	92	90	93	10.1

time, accelerates the recognition speed for the system. Figure 12 depicts the image after detection by the YOLOv8 model combined with the other backbones. The results indicate that all models are capable of clearly detecting major errors. However, for minor and blurry errors, the improvement in models such as YOLOv8 and YOLOv8+1p is limited, resulting in poor detection capabilities. The remaining models, on the other hand, are able to detect these errors effectively.

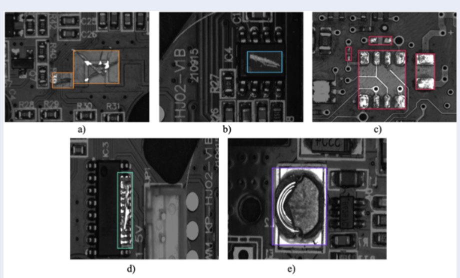

Figure 12: Types of defects on PCB: a) Scratches on the circuit board; b) Scratches on components; c) Missing/lost component; d) Damaged component pins; e) Faulty components.

The accuracy graph of the HRDnet+2 backbone model is depicted in Figure 13, illustrating that the training results of the model are relatively stable and converge after 50 epochs.

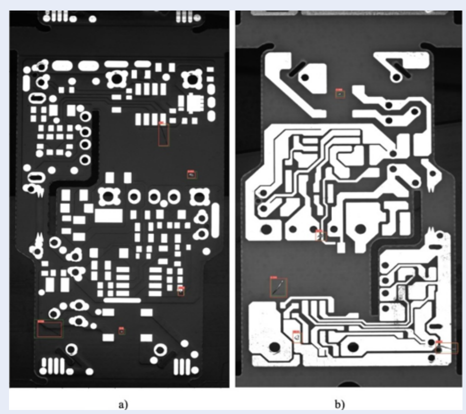

Figure 13: Results on bare PCBs: a) front side; b) back side

Figure 14 presents the recision–recall curves of the YOLOv8 model combined with the HRDNet-2 backbone. Classes 2 (missing/lost component) and 3 (damaged component pins) yield the highest AP values (0.972 and 0.971, respectively), while Class 0 (cratches on the circuit board) exhibits a lower AP (0.866), reflecting the greater difficulty associated with thin and low-contrast defects. The recision–

Table 5: The accuracy of the models on the test set.

Backbone	Parameters (M)	F1-score	Precision (%)	Recall (%)	mAP0.5 (%)
YOLOv8 original	3.2	50	91	85	91
YOLOv8-1P	4	50	92	87	92.5
HRNet48	67	50	94	88	94
ResNet152	61	50	89	88	92
HRDnet- 3back-bone	4.1	50	91	89	92.8
HRDnet- 2back-bone	3.8	50	92	90	93

recall curves maintain high precision over most of the recall range, indicating the effective control of false positives and a strong capability in detecting small defects, particularly with the integration of the HRDNet-2 backbone.

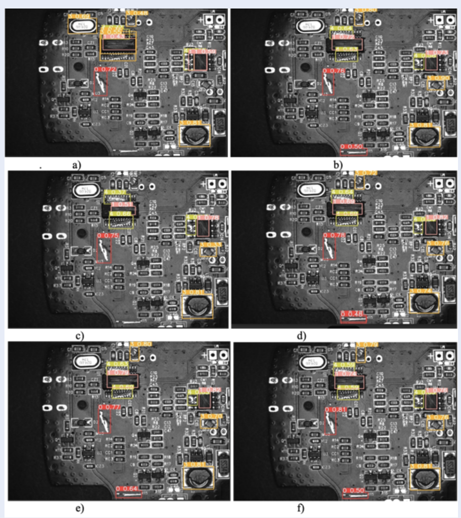

Figure 14: The results of identifying different types of errors on a PCB: a) Ground truth errors; b) Original YOLOv8; c) YOLOv8+1P; d) YOLOv8+ Resnet152; e)YOLOv8+HRNET48; f) HRDNet+2 backbone; g) HRD-Net+2 backbone.

The accuracy of each class in the combined YOLOv8 and HRDNet+2 backbone model is further illustrated through the confusion matrix in Figure 15. This matrix indicates the accuracy of each class on the test set and also demonstrates the consistent and high accuracy of the classes.

The identification of different types of errors on a PCB is presented in Figure 16. Figure 16(a) shows a PCB image with various types of errors, each framed with a corresponding color. Figure 16(b) displays the image

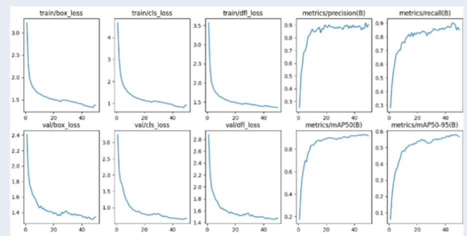

Figure 15: Loss and accuracy graph of the YOLOv8 model combined with HRDnet 2 backbone

after detection by the YOLOv8 model combined with the HRDNet+2 backbone. The results indicate that the model successfully identifies all types of errors, including small and complex ones, accurately classifying each error type.

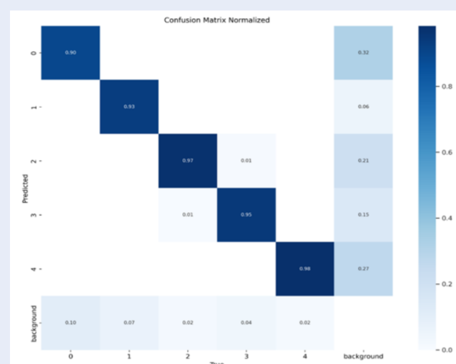

Figure 16: Confusion matrix of the YOLOv8 model combined with HRDnet 2 backbone on test set

Comparison With Other Datasets

We performed a comparison across popular datasets for PCB defect detection, as presented in Table 6.

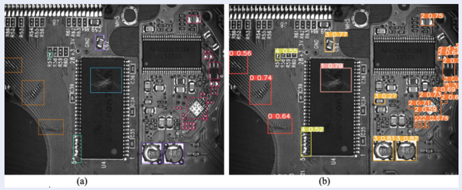

Figure 17: The results of identifying different types of errors on a PCB: a) Ground truth errors; b) The errors detected by the YOLOv8 model with HRDNet+2 backbone

Here, the authors of the papers have proposed error classification models to ensure high accuracy. However, the datasets are relatively limited, and the number of labeled errors is insufficient, which may lead to overfitting. Combining the two datasets may result in a decrease in accuracy. Meanwhile, we focused on constructing a diverse dataset, utilizing modern optical techniques to enhance the detection of complex errors. Simultaneously, we improved the model, selecting a model that not only meets accuracy requirements but also ensures a suitable size for real-time deployment in intrusion detection systems.

One should note that Table 6 summarizes the results reported in previous works on different public datasets; we did not train or evaluate our models directly on HRIPCB, PKU-Market-PCB, or Deep-PCB. Our dataset differs substantially from these benchmarks in both optical characteristics (coaxial monochrome imaging) and defect distributions. Consequently, cross-dataset evaluation would require careful domain adaptation and re-annotation, which lies beyond the scope of this study. Instead, Table 6 highlights the relative scale and diversity of our dataset compared with existing ones and underlines the need for optimized optical acquisition in addition to algorithmic improvements.

DISCUSSION

The results of this study provide several key insights into the integration of optical imaging and deep learning for PCB defect detection. One notable finding is the pronounced sensitivity of detection in terms of the image quality. Even with advanced neural architectures, insufficient contrast or poorly defined object boundaries can hinder performance. This reinforces the importance of designing acquisition systems that address the specific optical challenges posed by PCB surfaces, particularly in scenarios involving reflective coatings or densely packed components.

The comparative analysis between the backbone configurations reveals that architectural depth and multi-scale feature fusion directly influence the system's capacity to capture fine-grained defects. While models with greater complexity generally achieve higher detection rates, the trade-off in computational load suggests that deployment decisions must consider production line constraints. In this context, architectures that balance accuracy with inference speed can deliver practical value without compromising inspection throughput.

From a broader perspective, the study's approach bridges a gap between controlled laboratory performance and the operational demands of electronic manufacturing. Many prior works have reported high accuracy under constrained datasets but face performance degradation in real-world conditions due to dataset bias and limited variability. By combining a dataset enriched with defect diversity and an optical design tailored to manufacturing realities, this work moves closer to bridging that divide.

A more systematic robustness evaluation under intentionally perturbed lighting conditions offers an interesting direction for future work.

CONCLUSIONS

This study proposed a two-stage PCB defect detection framework combining an optimized coaxial illumination optical system with enhanced YOLOv8 backbones. The approach achieved high precision in detecting small, complex, and visually similar defects, with the YOLOv8 + HRDNet-2 backbone offering the optimal balance between accuracy and efficiency. The experimental results confirm that the method outperforms conventional approaches in terms of both detection performance and real-time capabilities, providing a practical solution for quality control in electronics manufacturing. Future research should explore adaptive model compression and knowledge distillation to further reduce computational requirements without eroding the quality of detection. Additionally, incorporating multimodal inspection data—such as combining optical imaging with X-ray or thermal scans—could enhance robustness against visually ambiguous defects. These directions would extend the applicability of defect detection systems beyond PCB inspection to other domains with similar visual challenges.

ABBREVIATIONS

The author needs to provide additional information.

Table 6: Comparison with other datasets.

Dataset	Total images	Number of defect	Model	Accuracy (%)
HRIPCB	1386	3003	Transformer-YOLO	96.5
PKU-Market-PCB	693	2953	TDD-Net	98.9
DeepPCB	1500	8853	GPP module	98.2
PKU-Market-PCB+ DeepPCB	2193	11806	DDTR	81
Our Dataset	3989	29851	Yolov8+2 HRDNet	93.8

COMPETING INTERESTS

The authors have not received any financial support from any person, institution, or organization for this research work. The authors declare that there are no conflicts of interest regarding the publication of this paper. The experiment data used to support the findings of this study are available from the corresponding author upon request. This research does not involve human and/or animal subjects. The image data of faulty circuit boards has been collected from various types of boards, captured through a real optical system. The model is built on training data and has been tested through the testing data set.

AUTHORS' CONTRIBUTIONS

Hieu Dau Sy and Thuan Tran Minh: Methodology, Design of the data acquisition system. Phuc Dang Thi and Tuan Le Tran Anh: Design the algorithm. All authors wrote sections of the manuscript and performed the final corrections. All authors have read and agreed to the published version of the manuscript.

ACKNOWLEDGEMENTS

This research is funded by Vietnam National University Ho Chi Minh City (VNU-HCM) under the grant number DS.C2025-20-17.

REFERENCES

1. Marques AC, Cabrera JM, Malfatti CF. Printed circuit boards: a review on the perspective of sustainability. J Environ Manage. 2013;131:298–306. Available from: https://doi.org/10.1016/j.jenvman.2013.10.003.
2. Magera JA, Dunn GJ, Google Patents. Printed circuit board. US Patent 7. 2008;459(202).
3. Moganti M, Ercal F, Dagli CH, Tsunekawa S. Automatic PCB inspection algorithms: A survey. Comput Vis Image Underst. 1996;63(2):287–313. Available from: https://doi.org/10.1006/cviu.1996.0020.
4. Anitha DB, Rao M. A survey on defect detection in bare PCB and assembled PCB using image processing techniques. In: 2017 2017 International Conference on Wireless Communications, Signal Processing and Networking (WiSPNET); 2017. p. 39–43. Available from: https://doi.org/10.1109/WiSPNET.2017.8299715.
5. Pal A, Chauhan S, Bhardwaj S. Detection of bare PCB defects by image subtraction method using machine vision. In: Proceedings of the World Congress on Engineering 2011 (WCE 2011); 2011. p. 2.
6. Aggawral N, Deshwal M, Samant P. A survey on automatic printed circuit board defect detection techniques; 2022. Available from: https://doi.org/10.1109/ICACITE53722.2022.9823872.
7. Thanh DT, Nam PT, Phuong NT, Que X, Anh NV, Hoang T, et al. Controlling the electrodeposition, morphology and structure of hydroxyapatite coating on 316L stainless steel. Mater Sci Eng C. 2013;33(4):2037–45. Available from: https://doi.org/10.1016/j.msec.2013.01.018.
8. Ling Q, Isa NA. Printed circuit board defect detection methods based on image processing, machine learning and deep learning: A survey. IEEE Access. 2023;11:15921–44. Available from: https://doi.org/10.1109/ACCESS.2023.3245093.
9. Sundaraj K. PCB inspection for missing or misaligned components using background subtraction. WSEAS Trans Inf Sci Appl. 2009;6:778–87.
10. Silva HG, Amaral TG, Dias OP. Automatic optical inspection for detecting defective solders on printed circuit boards.; 2010. Available from: https://doi.org/10.1109/IECON.2010.5675520.
11. Kim NH, Pyun JY, Choi KS, Choi BD, Ko SJ. Real-time inspection system for printed circuit boards.; 2001. Available from: https://doi.org/10.1109/ISIE.2001.931775.
12. Bai X, Fang Y, Lin W, Wang L, Ju BF. Saliency-based defect detection in industrial images by using phase spectrum. IEEE Trans Industr Inform. 2014;10(4):2135–45. Available from: https://doi.org/10.1109/TII.2014.2359416.
13. Wan Y, Gao L, Li X, Gao Y. Semi-supervised defect detection method with data-expanding strategy for PCB quality inspection. Sensors (Basel). 2022;22(20):7971. Available from: https://doi.org/10.3390/s22207971.
14. Lim D, Kim YG, Park TH. SMD classification for automated optical inspection machine using convolution neural network. In: 2019 Third IEEE International Conference on Robotic Computing (IRC); 2019. p. 395–8. Available from: https://doi.org/10.1109/IRC.2019.00072.
15. Wang C, Huang G, Huang Z, He W. Conditional transGAN-based data augmentation for PCB electronic component inspection. Comput Intell Neurosci. 2023;2023(1). Available from: https://doi.org/10.1155/2023/2024237.
16. Hu B, Wang J. Detection of PCB surface defects with improved faster-RCNN and feature pyramid network. IEEE Access. 2020;8:108335–45. Available from: https://doi.org/10.1109/ACCESS.2020.3001349.
17. Chen S, Liang X, Jiang W. PCB defect detection based on image processing and improved YOLOv5. J Phys Conf Ser. 2023;2562(1). Available from: https://doi.org/10.1088/1742-6596/2562/1/012002.
18. Chang CH, Chen HW, Lin CC. Detecting multiclass defects of printed circuit boards in the molded-interconnect-device manufacturing process using deep object detection networks. In: 2022 IEEE International Conference on Industrial Engineering and Engineering Management (IEEM); 2022. p. 1536–40. Available from: https://doi.org/10.1109/IEEM55944.2022.9989934.

19. Ebayyeh AA, Mousavi A. A review and analysis of automatic optical inspection and quality monitoring methods in electronics industry. IEEE Access. 2020;8:183192–271. Available from: https://doi.org/10.1109/ACCESS.2020.3029127.
20. He X, Malaiya Y, Jayasumana AP, Parker KP, Hird S. Principal component analysis-based compensation for measurement errors due to mechanical misalignments in PCB testing. In: 2010 IEEE International Test Conference. (2010); 2010. p. 1–10. Available from: https://doi.org/10.1109/TEST.2010.5699249.
21. Leta FR, Feliciano FF. Computational system to detect defects in mounted and bare PCB based on connectivity and image correlation. In: and others, editor. 2008 15th International Conference on Systems, Signals and Image Processing. (2008); 2008. p. 331–334. Available from: https://doi.org/10.1109/IWSSIP.2008.4604434.
22. Sani A, Pratama RS. Oxidation detection on PCB using image processing. In: and others, editor. 2020 3rd International Conference on Applied Engineering (ICAE); 2020. Available from: https://doi.org/10.1109/ICAE50557.2020.9350559.
23. Crispin A, Rankov V. Automated inspection of PCB components using a genetic algorithm template-matching approach. Int J Adv Manuf Technol. 2007;35(3-4):293–300. Available from: https://doi.org/10.1007/s00170-006-0730-0.
24. Ulger F, Yuksel SE, Yilmaz A. Anomaly detection for solder joints using B-VAE. IEEE Trans Compon Packaging Manuf Technol. 2021;11(12):2214–21. Available from: https://doi.org/10.1109/TCPMT.2021.3121265.
25. Wu H, Zhang X, Xie H, Kuang Y, Ouyang G. Classification of solder joint using feature selection based on Bayes and support vector machine. IEEE Trans Compon Packaging Manuf Technol. 2013;3(3):516–22. Available from: https://doi.org/10.1109/TCPMT.2012.2231902.
26. Deng YS, Luo AC, Dai MJ. Building an automatic defect verification system using deep neural network for PCB defect classification. In: and others, editor. 2018 4th International Conference on Frontiers of Signal Processing (ICFSP); 2018.
27. Haochen L, Bin Z, Xiaoyong S, Yongting Z. CNN-based model for pose detection of industrial PCB. In: and others, editor. 2017 10th International Conference on Intelligent Computation Technology and Automation (ICICTA); 2017. p. 390–393. Available from: https://doi.org/10.1109/ICICTA.2017.93.
28. Li YT, Guo JI. VGG-16 based faster RCNN model for PCB error inspection in industrial AOI applications. In: 2018 IEEE International Conference on Consumer Electronics-Taiwan (ICCE-TW); 2018. p. 1–2. Available from: https://doi.org/10.1109/ICCE-China.2018.8448674.
29. Chen W, Huang Z, Mu Q, Sun Y. PCB defect detection method based on transformer-YOLO. IEEE Access. 2022;10:129480–9. Available from: https://doi.org/10.1109/ACCESS.2022.3228206.
30. Li CJ, Qu Z, Wang SY, Bao KH, Wang SY. A method of defect detection for focal hard samples PCB based on extended FPN model. IEEE Trans Compon Packaging Manuf Technol. 2022;12(2):217–27. Available from: https://doi.org/10.1109/TCPMT.2021.3136823.
31. Ren S, He K, Girshick RB, Sun J. Faster R-CNN: towards real-time object detection with region proposal networks. arXiv. 2015;.
32. Ding R, Dai L, Li G, Liu H. TDD-Net: A tiny defect detection network for printed circuit boards. CAAI Trans Intell Technol. 2019;4(2):110–6. Available from: https://doi.org/10.1049/trit.2019.0019.
33. Xin H, Chen Z, Wang B. PCB electronic component defect detection method based on improved YOLOv4 algorithm. J Phys Conf Ser. 2021;1827(1). Available from: https://doi.org/10.1088/1742-6596/1827/1/012167.
34. Li J, Gu J, Huang Z, Wen J. Application research of improved YOLO v3 algorithm in PCB electronic component detection. Appl Sci (Basel). 2019;9(18):3750. Available from: https://doi.org/10.3390/app9183750.
35. Reis D, Kupec J, Hong J, Daoudi A. Real-time flying object detection with YOLOv8. 2023;.
36. Redmon J, Farhadi A. YOLOv3: an incremental improvement. arXiv. 2018;.
37. He K, Zhang X, Ren S, Sun J. Deep residual learning for image recognition. arXiv. 2015;.
38. Wang J, Sun K, Cheng T, Jiang B, Deng C, Zhao Y, et al. Deep high-resolution representation learning for visual recognition. arXiv. 2019;.
39. Liu Z, Gao G, Sun L, Fang Z. HRDNet: high-resolution detection network for small objects. arXiv. 2020;.
40. Huang W, Wei P. A PCB dataset for defects detection and classification. CoRR. 2019;.
41. Bhattacharya A, Cloutier SG. End-to-end deep learning framework for printed circuit board manufacturing defect classification. Sci Rep. 2022;12(1):12559. Available from: https://doi.org/10.1038/s41598-022-16302-3.
42. Tang S, He F, Huang X, Yang J. Online PCB defect detector on a new PCB defect dataset. CoRR. 2019;.
43. Feng B, Cai J. PCB defect detection via local detail and global dependency information. Sensors (Basel). 2023;23(18):7755. Available from: https://doi.org/10.3390/s23187755.
44. Lenhardt K. Optical systems in machine vision. In: and others, editor. In: Handbook of Machine and Computer Vision. John Wiley Sons Ltd; 2017. p. 179–290. Available from: https://doi.org/10.1002/9783527413409.ch4.
45. Ren Z, Fang F, Yan N, Wu Y. State of the art in defect detection based on machine vision. Int J Precis Eng Manuf Green Eng. 2022;9(2):661–91. Available from: https://doi.org/10.1007/s40684-021-00343-6.
46. Simonyan K, Zisserman A. Very deep convolutional networks for large-scale image recognition. arXiv. 2014;.
47. Szegedy C, Liu W, Jia Y, Sermanet P, Reed SE, Anguelov D, et al. Going deeper with convolutions. . arXiv. 2014;.
48. Dau SH, Dang TP, Han DQ, Hy TC, Khang LN, Dat KN. Optical design for automatic inspection system of defects on disposable surgical scalpel blades using machine vision, editors. In: 9th International Conference on the Development of Biomedical Engineering in Vietnam (BME 2022). vol. Vol. 95. Cham: Springer; 2024. p. 657–66. Available from: https://doi.org/10.1007/978-3-031-44630-6_54.
49. Tan M, Le QV. EfficientNet: rethinking model scaling for convolutional neural networks. . arXiv. 2019;.